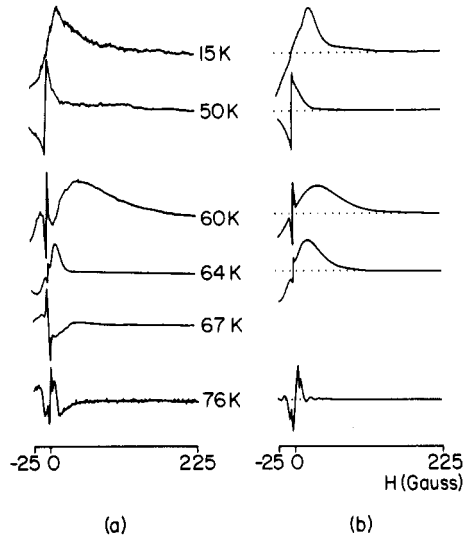

Figure 6. Comparison of LFMA line shapes observed for a $Bi_2Sr_2CaCu_2O_x$ crystal with magnetic field parallel to the c axis (a) with calculated curves (b). The signal observed at 67 K cannot be reproduced by calculation because of the phase reversal around 0 G. The modulation amplitude was 1 G, and microwave power was 1 mW.

distribution of H_0 values. In a crystal, H_0 should exhibit different fixed values with a narrower distribution for different types of Josephson junctions which might be related to different types of crystal defects. Hence, normalized superpositions of two or more diffraction formulas with different H_0 distributions were used as a reduction factor for the superconducting current versus magnetic field.

The parameters used in the calculations for Figure 6 are as follows. At 15 K $\eta_0 = 50$ and $F(H)$ is a superposition of 11 diffraction formulas with $H_0 = 5$–55 G (step 5 G) and a distribution of $\Delta H_0 = \pm 0.4 H_0$ for each. At 50 K $\eta_0 = 5$ and $F(H)$ is a superposition of eight diffraction formulas with $H_0 = 2$–30 G (step 4 G) and a distribution of $\Delta H_0 = \pm 0.8 H_0$ for each. At 60 K $\eta_0 = 3$ and $F(H)$ is a superposition of an envelope with $H_0 = 50$ G and relative amplitude 20 with a diffraction formula for $H_0 = 2$ G with $\Delta H_0 = \pm H_0$ and relative amplitude 1. At 64 K $\eta_0 = 3$ and $F(H)$ is a superposition of an envelope with $H_0 = 30$ G and relative amplitude 40 with a diffraction formula for $H_0 = 2$ G with $\Delta H_0 = \pm H_0$ and relative amplitude 1. At 76 K $\eta_0 = 1$ and $F(H)$ is the superposition of two diffraction formulas with H_0 equal to 12.5 and 5 G with $\Delta H_0 = \pm 0.1 H_0$ for both and a ratio of amplitudes equal to 3.

Conclusions

The Dulcic et al. model for the LFMA line shape can be satisfactorily applied to $YBa_2Cu_3O_x$ and $Bi_2Sr_2CaCu_2O_x$ superconductors. Most significantly, it accounts for the differences in the response of these two superconductor systems. Interpretation of the lack of hysteresis for the Bi compound suggests that the assumption $I_M \ll I_0$ is not met and leads to the conclusion that the Josephson junctions are more weakly coupled in $Bi_2Sr_2CaCu_2O_x$ than in $YBa_2Cu_3O_x$.

Acknowledgment. This research is supported by the Texas Center for Superconductivity at the University of Houston under the prime grant MDA-972-88-G-0002 from the Defense Advanced Research Projects Agency and by the State of Texas.

Registry No. $YBa_2Cu_3O_x$, 107539-20-8; $Bi_2Sr_2CaCu_2O_x$, 114901-61-0.

Thermal Generation of CH_3·(g) from CH_3OH Adsorbed on Oxygen-Covered Mo(110). C–O Bond Strength Considerations from Molecular Orbital Theory

Paul Shiller and Alfred B. Anderson*

Chemistry Department, Case Western Reserve University, Cleveland, Ohio 44106 *(Received: August 20, 1990)*

By use of the atom superposition and electron delocalization molecular orbital theory and a surface cluster model, it is found that O atoms (formally O^{2-}) and CH_3O bind most strongly on the highest coordination site of Mo(110). Compared to the 3.7-eV strong C–O bond in methanol formed by binding CH_3· and OH·, the forming of a methoxy anion by binding CH_3· to O^{2-} on the Mo surface generates an electron that is promoted to the surface conduction band, and this promotion weakens the C–O bond strength to about 1.4 eV. This explains the thermal desorption results of Serafin and Friend, who observed CH_3·(g) formation on heating a Mo(110) surface with adsorbed methoxy to 590 K.

Introduction

Methanol adsorption and decomposition on clean metal surfaces has been studied extensively. Experimental results have been reported for copper,[1-4] nickel,[5,6] platinum,[7-9] palladium,[10-12] molybdenum,[13-17] ruthenium,[18] iron,[19-21] rhodium,[22,23] and tungsten.[15] On clean late transition metal surfaces methanol forms a stable methoxy intermediate which decomposes to CO and H_2

(1) Kojima, I.; Sughara, H.; Miyazaki, E.; Yasumuri, I. *J. Chem. Soc., Faraday Trans. 1* **1981**, *77*, 1315.
(2) Wachs, I. E.; Madix, R. J. *J. Catal.* **1978**, *53*, 208.
(3) Sexton, B. A.; Hughes, A. E.; Avery, N. R. *Surf. Sci.* **1985**, *155*, 366.
(4) Hoffman, P.; Menzel, D. *Surf. Sci.* **1987**, *191*, 353.
(5) Bare, S. R.; Stroscio, J. A.; Ho, W. *Surf. Sci.* **1985**, *150*, 399.
(6) Gates, S. M.; Russell, J. N.; Yates, Jr., J. T. *Surf. Sci.* **1984**, *146*, 199.
(7) Sexton, B. A.; Rendulic, K. D.; Hughes, A. E. *Surf. Sci.* **1982**, *121*, 181.
(8) Sexton, B. A. *Surf. Sci.* **1981**, *102*, 271.
(9) Ehlers, D. H.; Spitzer, A.; Luth, H. *Surf. Sci.* **1985**, *160*, 57.
(10) Gates, J. A.; Kesmodel, L. L. *J. Catal.* **1983**, *83*, 437.
(11) Christman, K.; Demuth, J. E. *J. Chem. Phys.* **1983**, *76*, 6308.
(12) Levis, R. J.; Zhicherg, J.; Winograd, N. *J. Am. Chem. Soc.* **1989**, *111*, 4605.
(13) Miles, S. L.; Bernasek, S. L.; Gland, J. L. *J. Electron Spectrosc. Relat. Phenom.* **1983**, *29*, 239.
(14) Miles, S. L.; Bernasek, S. L.; Gland, J. L. *J. Phys. Chem.* **1983**, *87*, 1626.
(15) Benziger, J. B.; Preston, R. E. *J. Phys. Chem.* **1985**, *89*, 5002.
(16) Ko, E. I.; Madix, R. J. *Surf. Sci.* **1981**, *112*, 373.
(17) Serafin, J. G.; Friend, C. M. *J. Am. Chem. Soc.* **1989**, *111*, 8967.
(18) DePaola, R. A.; Hrbek, J.; Hoffman, F. M. *Surf. Sci.* **1986**, *169*, L348.
(19) Benziger, J. B.; Madix, R. J. *J. Catal.* **1980**, *65*, 36.
(20) Albert, M. R.; Lu, J.-P.; Bernasek, S. L.; Dwyer, D. J. *Surf. Sci.* **1989**, *221*, 197.
(21) Lu, J.-P.; Albert, M.; Bernasek, S. L.; Dwyer, D. S. *Surf. Sci.* **1989**, *218*, 1.
(22) Solymosi, F.; Berkő, A.; Tarnóczi, *Surf. Sci.* **1984**, *141*, 533.
(23) Solymosi, F.; Tarnóczi, T. I.; Berkő, A. *J. Phys. Chem.* **1984**, *88*, 6170.

0022-3654/91/2095-1396$02.50/0

TABLE I: Parameters Used in the Calculations: Principal Quantum Number, n; Orbital Ionization Potential, IP (eV); Slater Orbital Exponents, ζ (au); and Coefficients for Double-ζ d Functions, c

	s			p			d					
atom	n	IP	ζ	n	IP	ζ	n	IP	c_1	ζ_1	c_2	ζ_2
H	1	11.60	1.200									
C	2	14.59	1.6583	2	9.26	1.6180						
O	2	26.48	1.9460	2	11.62	1.9270						
Mo	5	9.10	2.2560	5	5.92	1.9560	4	10.06	0.5898	4.5420	0.5898	1.9010

on heating to ~300 K. Copper seems to be the only exception in that the decomposition appears to pass through a stable formaldehyde intermediate. On early transition metals the decomposition products are H_2 and adsorbed C and O.

Methanol adsorption and decomposition are affected by adsorbed oxygen atoms. Miles et al.[13] found that methanol desorbs intact from a fully oxygen covered surface. Ko and Madix[16] found significant changes in activity and selectivity for the reactions of formaldehyde and methanol over W and Mo(100) surfaces when covered with oxygen. Solymosi et al. found methoxy to be stabilized on O-covered Rh(111).[23] It is thought that oxygen adatoms stabilize the methoxy intermediate by blocking active bare metal sites that are necessary for complete methyl group dehydrogenation. In the case of methanol adsorption on oxygen-covered Fe, Lu et al.[21] found a formaldehyde intermediate; on the clean surface decomposition was complete. This implies that adsorbed O allowed the loss of one methyl H from the methoxy intermediate and stabilized formaldehyde against dehydrogenation. It should be noted that it is not known at what stage the CO bond is broken during methoxy or formaldehyde decomposition in these studies.

Cleavage of the C–O bond in surface methoxide anions is also possible. It appears that the carbon to oxygen bond can be very weak when a methyl radical is bound to an oxide. This is apparent from observations that gas-phase methyl radicals are generated by H abstraction from CH_4 over SiO_2, Al_2O_3, Bi_2O_3, and MgO.[24] Mehandru et al.[25] used molecular orbital theory to suggest that methyl radicals bind weakly to the anion planes of layered MoO_3 and are mobile over them, a consequence of destabilization caused by the promotion of the methyl radical electron to the metal valence conduction band according to

$$CH_3\text{•}(g) + O^{2-}(s) \rightarrow CH_3O(s) + e^-(cb) \quad (1)$$

At O^- defect sites CH_3• binds strongly as methoxide.

Serafin and Friend recently observed the generation of gas-phase methyl radicals on heating a Mo(110) surface with adsorbed methoxide. The maximum CH_3• desorption rate was at about 590 K.[17] The surface was prepared by first precovering with about 1/3 monolayer of atomic oxygen and then introducing methanol which dissociatively adsorbed:

$$CH_3OH(g) + O(ads) \rightarrow CH_3O(ads) + OH(ads) \quad (2)$$

The adsorbed O and OH, along with CH_3O(ads) decomposition products, were believed to help stabilize some of the CH_3O(ads) against dehydrogenation, and these methoxide groups were the source of CH_3•(g). There is also evidence that neighboring atoms on the surface can serve to weaken C–O bonds in oxygenates bound to the surface through O. Serafin and Friend found the decomposition of ethylene oxide chemisorbed on Mo(110) to C_2H_4(g) and O(ads) was selectively enhanced by coadsorbed O.[26]

The generation of CH_3•(g) from CH_3O(ads) with a maximum rate at 590 K implies, according to first-order desorption kinetics, that the C–O bond strength is only about 1.5 eV,[27] which is substantially reduced from its methanol value of 3.7 eV. This is still greater than the binding energy of CH_3• to O^{2-} on an oxide surface (eq 1), and it seems likely that the difference is a result of a difference in electron promotion energy, i.e., conduction band energy. The purpose of this paper is to explore this idea by using molecular orbital theory. The effect of coadsorbed O atoms on the C–O bond strength is also examined. A bulk superimposable cluster model of the Mo(110) surface is employed. The atom superposition and electron delocalization molecular orbital (ASED-MO) theory is used.

TABLE II: Calculated O–Mo Distances, R (Å), and Binding Energy, BE (eV), for O on Various Sites of Mo(110) Modeled by the Mo_{25} Cluster

site	R	BE
1-fold	1.66	5.32
short-bridge	1.72	6.23
long-bridge	1.74	6.58
3-fold	1.81,[a] 1.82[b]	6.92

[a] Distance from one Mo. [b] Distance from two Mo's.

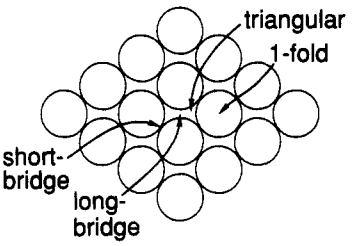

Figure 1. Mo_{25} cluster model of the (110) surface showing adsorption sites studied.

Method

In ASED-MO theory the electronic charge density of a molecule is partitioned into free-atom parts and the electron delocalization part which accompanies bond formation. As the atoms in a diatomic molecule come together the electrostatic forces on the nuclei can be integrated to give the Born–Oppenheimer potential energy, $E(R)$. The rigid-atom densities yield a repulsive component $E_D(R)$, and electron delocalization yields an attractive component, $E_R(R)$:

$$E(R) = E_R(R) + E_D(R) \quad (3)$$

For a polyatomic molecule the process is repeated. $E_D(R)$ is not available but it is well approximated by the binding energy calculated using a modified extended Hückel Hamiltonian, provided each atom pairwise contribution to $E_R(R)$ is evaluated by integrating the force on the nucleus of the less electronegative atom. Some previous applications of the method include the photoactivation of CH bonds in a coordinated methoxy in a molybdenum oxyanion,[28] the electronic properties of MoO_3,[29] and the activation of CH_4 by surface O^- and the binding of CH_3• to the MoO_3 surface.[25]

The atomic parameters used for Mo, O, C, and H (Table I) are those used previously, except the oxygen exponents in methoxy are increased 0.2 au, corresponding to a less negative charge compared to that of oxide anions. A two-layer-thick Mo_{25} cluster model of the (110) surface is used (Figure 1). Since neutron

(24) Driscoll, D. J.; Martir, W.; Wang, J.-X.; Lunsford, J. H. *J. Am. Chem. Soc.* **1985**, *107*, 58.
(25) Mehandru, S. P.; Anderson, A. B.; Brazdil, J. F.; Grasselli, R. K. *J. Phys. Chem.* **1987**, *91*, 2930.
(26) Serafin, J. G.; Friend, C. M. *J. Am. Chem. Soc.* **1989**, *111*, 6019.
(27) Redhead, P. A. *Vacuum* **1962**, *12*, 203.
(28) Anderson, A. B.; Ray, N. K. *J. Am. Chem. Soc.* **1985**, *107*, 253.
(29) Anderson, A. B.; Kim, Y.; Ewing, D. W.; Grasselli, R. K.; Tenhover, M. *Surf. Sci.* **1983**, *134*, 237.

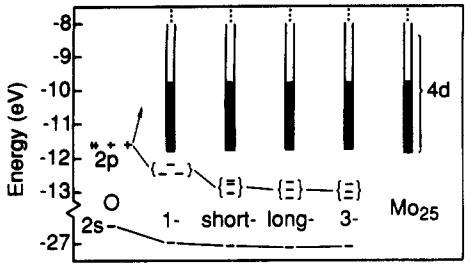

Figure 2. Bonding stabilizations for an oxygen atom binding at 1-fold, short-bridge, long-bridge, and 3-fold sites of the Mo_{25} cluster model.

TABLE III: Calculated C–O Bond Length, *R* (Å), and Binding Energy, BE (eV), of Methoxy Binding to Mo(110)

site	*R*	BE
1-fold	1.48	4.74
short-bridge	1.50	5.44
long-bridge	1.50	5.46
3-fold	1.50	5.55

TABLE IV: Calculated C–O Bond Length, *R* (Å), and Binding Energy, BE (eV), for $CH_3^\bullet$ Binding to O(ads) on Various Sites of the Mo_{25} Cluster

site	*R*	BE
1-fold	1.48	1.88
short-bridge	1.50	1.62
long-bridge	1.54	1.41
3-fold	1.54	1.41

diffraction yields no evidence for a substantial magnetic moment in Mo,[30] paired electron occupations are assigned to the d band.

Results

O and CH_3O Binding to Mo(110). For various sites of the O atom binding to the central region of the cluster shown in Figure 1, the calculated binding energies increased in the order 1-fold < short-bridge < long-bridge < 3-fold. Energies and O–Mo distances are given in Table II. The "3-fold site" does not actually possess triangular symmetry, and the O–Mo distances reflect this. The preference for the highest coordinate site is expected because the covalent overlap of the O 2p and Mo s + d band orbitals is the greatest there. As Figure 2 shows, there is a parallel between the O binding energies and the O 2p orbital stabilizations. The binding energy at the 1-fold site, 5.3 eV, is in reasonable agreement with the MoO diatomic value of 5.0 eV,[31] and the value at the 3-fold site is greater by 1.2 eV than the experimental surface value of 5.7 eV on polycrystalline Mo at ~0.5 monolayer coverage.[32]

Methoxy is calculated to also favor the 3-fold site, and binding energies are less than for O (Table III). Only for the long-bridge site did tilting the CO axis from the surface normal produce stability and the tilt was 3°, so in subsequent calculations the CO axis was fixed to be normal to the surface. The methoxy structure was taken from the calculated methanol structure, with the C–H distance, 1.21 Å, overestimated by 0.1 Å as is typical for the method and the OCH angles 106° compared to 113° for the experimental[32] structure. The calculated HOC angle in methanol is 25° larger than the experimental value of 109°, and the calculated C–O distance of 1.53 Å compares with the experimental value of 1.43 Å. The calculated OH distance is 1.02 Å compared to 0.96 Å from experiment. Most importantly, the CO dissociation energy is calculated to be 3.45 eV compared to the experimental value of 3.7 eV.

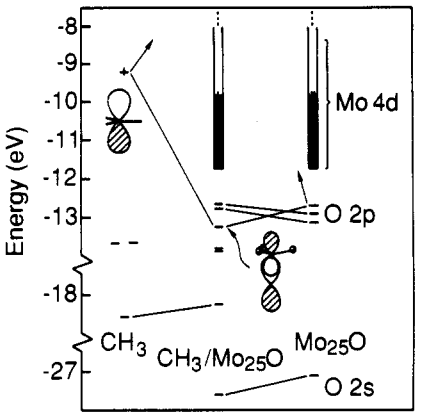

Figure 3. Bonding interactions between $CH_3^\bullet$ and oxygen atoms in the long-bridge site on the Mo_{25} cluster model.

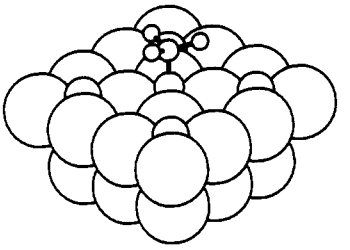

Figure 4. CH_3O on the long-bridge site in the presence of four oxygen atoms in triangular sites on the Mo_{25} cluster model.

$CH_3^\bullet$ Binding to an Adsorbed O Atom. In studying $CH_3^\bullet$ binding to O(ads), the position of the O atom is constrained at the above-calculated heights. The free methyl radical is planar, and when bound to O the methanol structure is used. Within this model the bond properties shown in Table IV are obtained. The C–O bond is strongest and shortest when CH_3O(ads) is on the 1-fold site and weakest and longest when it is on the long-bridge and 3-fold sites. In the latter sites the 1.41-eV $CH_3^\bullet$ binding energy is close to that expected for $CH_3^\bullet$ desorption from CH_3O(ads) at 590 K. Figure 3 shows the calculated C–O σ bond formation in the long-bridge case. There is also some net π repulsion between the doubly degenerate CH_3 σ orbitals and the O 2p + Mo orbitals in the surface plane. From one viewpoint, it is evident that the C–O bond in CH_3O(ads) is calculated to be about 2 eV weaker than in CH_3OH largely because of lessened charge-transfer stabilization of the $CH_3^\bullet$ radical orbital electron. On the surface this electron may be viewed as transferring to the Mo Fermi level, but in $CH_3^\bullet$ + $OH^\bullet$ it transfers to the $OH^\bullet$ radical orbital which is about 2.4 eV more stable. The remaining 0.4-eV difference is caused by the differences in orbital interactions between $CH_3^\bullet$ and O(ads) and $OH^\bullet$. Alternatively, it can be said that when the C–O bond forms between $CH_3^\bullet$ and O^{2-}, the energy of electron promotion to the surface conduction band causes the CO bond in CH_3O(ads) to be weak. The variations in C–O bond strengths correlate with the p_z orbital energy of surface O in the different sites. This orbital becomes more stable in the order 1-fold < short-bridge < long-bridge < 3-fold, which means it moves further from the higher lying $CH_3^\bullet$ radical orbital and, in the sense of perturbation theory, this progressively weakens the C–O bond.

$CH_3^\bullet$ Binding to an Adsorbed O Atom with Coadsorbed O. With four O atoms placed on 3-fold sites of the Mo_{25} cluster modeling 1/4 monolayer O coverage and CH_3O(ads) placed in a central long-bridge site as shown in Figure 4, the calculated C–O bond length is the same as when the four O (ads) are absent. However, the C–O bond strength is reduced by 0.09 eV in the presence of the four O. This establishes that the presence of coadsorbed O has a relatively small weakening effect on the C–O bond strength of CH_3O(ads).

(30) Rado, G. T.; Suhl, H., Eds. *Magnetism*; Academic: New York, 1963; p 225.

(31) Huber, K. P.; Herzberg, G. *Molecular Structure and Molecular Spectroscopy. Constants of Diatomic Molecules*; Van Nostrand and Reinhold: New York, 1979.

(32) Greaves, W.; Stickney, R. E. *Surf. Sci.* **1968**, *11*, 395.

(33) *CRC Handbook of Chemistry and Physics*, 67th ed.; CRC Press: Boca Raton, FL, 1986–1987.

Conclusions

Our calculations indicate that O(ads) and CH_3O(ads) both become increasingly stable as the O increases its coordination from 1-fold to short-bridge to long-bridge to 3-fold on the Mo(110) surface. In all cases the C–O bond in CH_3O(ads) is weak because of electron promotion to the surface Fermi level as in eq 1, and it becomes progressively weaker as O goes from low coordination to high coordination because the surface O $2p_z$ orbital energy level is shifted further away from resonance with the $CH_3^\bullet$ radical orbital energy level, which weakens the C–O σ bonding stabilization. The calculated C–O bond strength of 1.3–1.4 eV in CH_3O(ads) is consistent with the 590 K thermal desorption maximum for $CH_3^\bullet$ observed by Serafin and Friend. In the case of nondefective oxides $CH_3^\bullet$ binds even more weakly to surface O^{2-} because electron promotion attendant to C–O bond formation is to higher lying cation conduction bands. For oxides with low-lying bandgap cation surface states, such as Bi_2O_3,[34] the $CH_3^\bullet$ adsorption energy to O^{2-} may be expected to be higher than would be anticipated from the bulk O 2p to cation bandgap. The binding of $CH_3^\bullet$ to O(ads) on other metal surfaces will be expected to increase in strength as a function of increased Fermi level stability.

Acknowledgment. This research was supported by a grant from the Gas Research Institute.

Registry No. Mo, 7439-98-7; O, 17778-80-2; $MeO^\bullet$, 2143-68-2; $CH_3^\bullet$, 2229-07-4.

(34) Mehandru, S. P.; Anderson, A. B.; Brazdil, J. F. *J. Chem. Soc., Faraday Trans.* **1987**, *83*, 463.

Effects of Molecular Conformation on the Packing Density in the Liquid State. 2. Effect of Attractive Forces

Masaharu Ohba† and Hiroyasu Nomura*

Department of Chemical Engineering, School of Engineering, Nagoya University, Chikusa-ku, Nagoya, 464 Japan *(Received: March 13, 1990)*

The differences of some thermodynamic quantities in cis and trans conformers for model fluids at constant pressure have been calculated by use of the high-temperature approximation. A fluid composed of tetraatomic fused hard spheres is taken as a reference system, and its properties are obtained from the PY-like integral equation of RISM-1. It is found that the differences of volumetrical properties in cis and trans conformers for several compounds such as hydrocarbons, haloalkenes, and alcohols are well described by this theory. The difference of the heat of vaporization in cis and trans conformers estimated is in fairly good agreement with that for liquid hydrocarbons, while for alcohols the agreement is poor. This implies that the volumetrical properties are predominantly determined by the repulsive force for almost all liquids; on the other hand, for the heat of vaporization, the attractive force plays an important role, especially, for substances with strong attractive forces such as alcohols.

Effects of the conformational change of molecules on the local structure and thermodynamic properties of liquids are of fundamental interest to many areas of physical chemistry. For example, the study of conformational equilibria of rotational isomers in the liquid phase has been carried out by several authors.[1-4] These effects appear most explicitly in the thermodynamic properties of neat liquids of cis and trans conformers, respectively.

The general trend is found in the difference of volumetrical properties (the density, the compressibility, etc.) of neat liquids between cis and trans conformers. For example, the density of cis conformers is larger than that of trans conformers for almost all cases. In a previous paper[5] (part 1 of this study, hereafter referred to as I), we investigated the structure and properties of fluids composed of tetraatomic fused hard spheres and showed that this trend can be essentially explained by the packing effect of molecules, that is, by the repulsive term of intermolecular forces. In I, we restricted our concern to volumetrical properties only. However, a similar tendency is also found in the difference of the energetic properties between cis and trans conformers, though it is not so general as the case of volumetrical properties. For example, for hydrocarbons the heat of vaporization, ΔH_v, of the cis conformer is larger than that of the trans conformer.

The purpose of this work is to explain the above-mentioned trend including that of the energetic properties. For this purpose, we have calculated the effect of the attractive force upon thermodynamic properties of the cis and trans conformers by the use of the first-order perturbation theory (the high-temperature approximation, HTA), which gives good results for a high-density fluid.[6] In HTA, the correction terms of thermodynamic properties due to the attractive force are calculated by using the radial distribution functions of the reference system where only the repulsive potential is assumed in our calculations. Thus, the correction terms of thermodynamic properties calculated by this theory is essentially controlled by the shape of molecules. Comparison of the theoretical and experimental results has clarified successfully the difference of the role of the repulsive force and the attractive force for each substance.

In the calculations of I, the pressure evaluated is unrealistic, because of neglect of the internal pressure arising from the attractive force. As a result, the condition of constant pressure used in I is somewhat artificial. This problem is resolved by considering the attractive force. This is also one of the purposes of this work.

In the next section, the models and the method of calculations will be described. The calculated dependences of $\rho k_B T \kappa \tau$ and ΔH_v on η have been compared with experimental results, and the differences of the thermodynamic properties between the cis and trans conformers have also been investigated. Finally, in the case of polyatomic molecular fluids, the relation between HTA and

† Present address: Kawaijuku Educational Institution.
* To whom correspondence should be addressed.

(1) Nomura, H.; Udagawa, Y.; Murasawa, K. *J. Mol. Struct.* **1985**, *126*, 229. Nomura, H., Koda, S. *Bull. Chem. Soc. Jpn.* **1985**, *58*, 2917. Nomura, H.; Koda, S.; Hamada, K. *J. Chem. Soc., Faraday Trans. 1* **1987**, *83*, 527; *Ibid.* **1988**, *84*, 1267.
(2) Pratt, L. R.; Hsu, C. S.; Chandler, D. *J. Chem. Phys.* **1978**, *68*, 4202. Hsu, C. S.; Pratt, L. R.; Chandler, D. *J. Chem. Phys.* **1978**, *68*, 4213.
(3) Zichi, D. A.; Rossky, P. J. *J. Chem. Phys.* **1986**, *84*, 1712.
(4) Enciso, J. A.; Almarza, N. G.; Bermejo, F. J. *J. Chem. Phys.* **1989**, *90*, 413; *Ibid.* **1989**, *90*, 422.
(5) Nomura, H.; Ohba, M. *J. Phys. Chem.* **1989**, *93*, 8101.
(6) Barker, J. A.; Henderson, D. *J. Chem. Phys.* **1967**, *47*, 2856.

0022-3654/91/2095-1399$02.50/0